DOE-ER45460-1

DEVELOPING IMPROVED RELATIONSHIPS BETWEEN MICROSTRUCTURE AND CREEP AND SHRINKAGE OF CEMENT-BASED MATERIALS

Final Report

Professor Hamlin M. Jennings

Northwestern University

Evanston, IL 60208

Report Period: September 9, 1998 – July 31, 2000

Prepared for

THE U.S. DEPARTMENT OF ENERGY

AGREEMENT NO. DE-FG02-91ER45460

DISCLAIMER

1 Overview of Recent Research

The research during the final phase of this project led to significant advancements in our understanding of the colloidal nature of calcium silicate hydrate (C-S-H) in cement paste. There were several research areas that contributed to this progress. Examination of the drying shrinkage deformations in cement pastes by the Deformation Mapping Technique (DMT) revealed strong similarities in the drying behavior of C-S-H and other colloidal materials. Reassessment of the reported values of surface area and porosity of C-S-H lead to the conclusion that C-S-H exists in a low density and high density structure, the former being the only structure that is detected in nitrogen sorption. Small angle neutron scattering (SANS) investigations on C-S-H provided additional evidence for the existence of two C-S-H densities. Collectively, the DMT results and our refined understanding of the porous structure of C-S-H inspired a new model of C-S-H. The model envisions C-S-H as composed of colloidal precipitates of several nanometers in diameter that agglomerate into fractal structures of high or low density. The success of the model lies in its excellent ability to resolve apparent inconsistencies in reported values of specific surface area, density, pore volume and pore size that are measured by different experimental techniques.

Several published works have been produced by the present research. The references of these publications will be mentioned in their entirety in the body of the report.

2 Drying Shrinkage of Cement Paste as Measured by the Deformation Mapping Technique (DMT)

2.1 Deformation Mapping Technique (DMT)

The Deformation Mapping Technique (DMT) is a sophisticated image analysis algorithm that compares the grayscale intensities of two digital images, one corresponding to an unstressed

state, the other corresponding to a stressed state. Since the images are captured at the same physical location on the material of interest, the comparison of the grayscale intensities of the two images allows quantification of the relative deformation in each pixel of the stressed image. Results of deformation throughout the digitized microstructure can be expressed either in the form of deformation maps, where the spatial arrangement of compactions (analogous to a compressive strains) and rarefactions (analogous to a tensile strains) are displayed as an image, or in the form of deformation histograms, where the distribution of deformation intensity can be assessed.

It is important to note that our initial measurements of deformation simply measured the *average* deformation in a stressed image by examining the change in distance between several pairs of points in both images. While this technique provides an estimate of the average deformation in the microstructure, it does not provide information about the distribution of local deformation within the digitized microstructure. The DMT algorithm was thus improved upon to calculate the principal deformations in each pixel of the stressed image. The mathematics involved in computing the principal deformations on a pixel basis have recently been published ([1]: Neubauer, C.M., Garboczi, E.J., Jennings, H.M., *The Use of Digital Images to Determine Deformation Throughout a Microstructure*, J. Mater. Sci., 35(22), 2000, p. 5741-5749.); the good agreement between the DMT and well-established finite element algorithms on simulated images clearly indicates the excellent accuracy of the DMT.

2.1 Drying shrinkage of cement paste at varying relative humidities

The Deformation Mapping Technique (DMT) has been highly successful in studying the drying shrinkage of cement-based materials. One of the goals of recent DMT investigations ([2]: Neubauer, Jennings, H.M., *The Use of Digital Images to Determine Deformation Throughout a*

Microstructure , Part II: Application to Cement Paste, J. Mater. Sci., **35** (22), 2000, p. 5751-5765) was to examine the progressive deformation responses of cement paste as it is dried from saturation. According to the classic results of Roper [3], cement paste undergoes a series of distinct drying shrinkage mechanisms as the paste is equilibrated at successively lower relative humidities. Conventionally, drying shrinkage is divided into four regions: (1) Drying to 90% rh produces a relatively small shrinkage for the amount of water evaporated since the emptying of large capillaries produces negligible stress. (2) Further drying to 40% rh produces a significantly larger shrinkage for the amount of water evaporated since the emptying of smaller capillaries and gel pores produces larger stresses. (3) Drying from 40% to 20% rh produces relatively little shrinkage that is often attributed to the loss of adsorbed water. (4) Drying below 20% rh is accompanied by the loss of interlayer water, causing irreversible collapse of the C-S-H structure.

2.1.1 Experimental procedure

Cement pastes were prepared by hand mixing a Type I cement with de-ionized water for 5 minutes, placing them on a rolling mill overnight to prevent sedimentation prior to hardening, and then storing them in lime water baths at the appropriate temperature until testing age.

Once a sample reached the desired age, it was removed from the water bath and broken apart using a hammer. Several flakes approximately 1 cm^2 x 1 mm were collected and placed in the specimen chamber of the environmental scanning electron microscope (ESEM) at the initial relative humidity (90% RH) and allowed to equilibrate for approximately 30 minutes. It was determined that 30 minutes was more than sufficient a period of time for deformation to occur and the sample to stabilize (10-15 minutes was actually adequate). Images of selected areas were taken. Then the relative humidity in the chamber was dropped to the next lower level and again

allowed to equilibrate for approximately 30 minutes before new images of the selected areas were acquired. This process was repeated for all of the desired relative humidities.

To relate our results to those of Roper [3], two cement paste samples, with w/c = 0.35 and w/c = 0.50 were aged for 7 days at room temperature. Images were collected at 90%, 80%, 75%, 55%, 35%, 25% (for the w/c = 0.50 sample only), and 20% RH (for the w/c=0.35 sample only). Using the 90% RH image as the reference unstressed image, deformation maps and distributions were produced at each lower RH value, using the DMT as described above and elsewhere [1]. The temperature in the specimen chamber was held constant at 10°C, and changes in relative humidity were controlled by changing the water vapor pressure in the specimen chamber. Each image was 512 x 512 pixels in size.

2.1.2 DMT results

The deformation maps for the 0.35 and 0.50 w/c cement pastes that were exposed to successively lower relative humidities are reported in Figures 1 and 2. Compactions and rarefactions are displayed in separate maps at each relative humidity to emphasize that drying shrinkage is a competition between both compactions and rarefactions at the micron scale. Upon further inspection, it becomes apparent that compactions and rarefactions form distinct morphologies. Below about 55% rh in both w/c ratios, the compactions cluster into localized regions while the rarefactions form crack-like networks that separate compaction regions. As the relative humidity is lowered down to 20%, the compaction regions coalesce into larger regions while the rarefactions become more intense and increasingly interconnected. At relative humidities above 75%, on the other hand, there is significantly less microscopic deformation in either sample, suggesting that larger capillaries are being emptied at this relative humidity range.

Shown in Figures 3 and 4 are the deformation histograms for the 0.35 and 0.50 w/c cement pastes, respectively. The histograms show higher levels of deformation in the 0.35 w/c sample as evidenced by its more pronounced shoulder on the compaction (i.e., deformations < 0%) side. The higher intensities of deformation can also be qualitatively seen in the deformation maps of Figures 1 and 2 where the 0.35 w/c sample possess noticeably darker deformations than the 0.50 w/c sample. However, when the compactions and rarefactions are averaged at each relative humidity, the average deformation in the field of view of the 0.35 w/c specimen is consistently lower (i.e., less negative) than that in the 0.50 w/c sample (see Table 1). It should be noted that the average deformations Table 1 are all less than 0%, indicating that there is a net compaction of the sample (i.e., the sample is shrinking). Collectively, these results indicate that the net microscopic deformation is higher in the more porous 0.50 sample while the local compactions and rarefactions are actually greater in the 0.35 w/c sample.

As shown above, bulk deformation is a competition between compactions and rarefactions. With this perspective in mind, insight can be obtained on phenomenon such as drying creep (i.e., the Picket effect). The greater than expected deformation that results from the non-linear coupling of simultaneous drying and loading is often explained by the presumption that the external load prevents the formation of cracks, which would otherwise relax the strained body and contribute a superimposed expansion on the net deformation. This theory, however, has never been confirmed with experimental evidence for the arrestment of crack formation during drying creep. One plausible explanation for this unresolved problem could lie in the fact that the features which contribute the expansive deformation in cement pastes are not necessarily macroscopic cracks. As seen in the DMT results above, expansive deformations in the form of rarefactions (which are presumably invisible precursors to microcracks) are inherently present in

the deformation of cement pastes, regardless of the formation of macroscopic cracks. Conceivably, the expansive component contributed by these rarefactions during drying could be nullified if an external compressive load was applied to the sample. This process would thereby cause the greater net compaction in the sample that is expected during the process of drying creep.

2.1.3 Similarities between the Drying of C-S-H and Colloidal Gels

An extremely vast array of materials fall under the broad category of colloidal gels. Essentially, these materials are linked by their porous structure, which creates a significant internal surface between a solid and fluid phase. The internal surface is so great that many of the phenomenon associated with colloidal gels are dominated by interfacial effects such as surface tension rather than bulk phase chemistry and physics which dictate other solids. The drying of colloidal gels is a good example of such a phenomenon since virtually all colloidal systems undergo a similar series of distinct stages during the evaporation of its fluid phase [4]. The initial period of drying is called the *constant rate period* since the decrease in volume of the gel is equal to the volume of liquid evaporated. Depending of the compliance of the solid network, volumetric contractions can reach an order of magnitude [5]. In a gel possessing a narrow pore size distribution, the liquid-vapor menisci remain at the surface of the shrinking gel during the constant rate period. The *critical point* marks the end of the constant rate period, as shrinkage is halted (since the network becomes too stiff) and cracking is most likely to occur. The *first falling rate period* is marked by an emptying of the pores of the gel by liquid flow. The *second falling rate period* is the final stage of drying where liquid can only escape from the body by diffusion of vapor to the surface.

The DMT results reported above suggest some interesting similarities between the drying behavior of C-S-H in cement pastes and other colloidal gels. The first issue concerns the issue of large local deformations. In Figures 3 and 4, the deformation histograms indicate that a substantial amount of pixels record compactions and rarefactions up to 40% to 50% during drying. It is believed that these large local deformations in the C-S-H structure are indicative of a drying colloidal gel during the constant rate period, where as mentioned earlier, the volumetric contraction can reach an order of magnitude. It should be noted that these large local deformations in the C-S-H are not detectable in a macroscopic bulk shrinkage measurement (as with calipers or other length measuring device) since they do not seem to contribute to the overall shrinkage of the sample. A closer analysis of the deformations in the histograms of Figures 3 and 4 indicate that the summations of the large deformations less than –6% and greater than +6% were consistently near zero (i.e., large compactions and rarefactions nullify each other). It is only the small deformations that record between approximately –6% to +6% deformation that actually contribute to the net deformations that are recorded in Table 1. These findings are good evidence that the large deformations are not a result of noise[1] or other artifacts in the digital image. In fact, the existence of large local deformations in colloidal systems have been observed qualitatively in the form of curling and crumpling during drying in transmission electron microscope investigations [4]. Moreover, large local deformations could also suggest a collapse of some of the C-S-H structure, which is an often cited mechanism for irreversible shrinkage in cement pastes.

Other similarities in the drying behavior of C-S-H with colloidal gels were seen at relative humidities below 35% rh. The 0.35 w/c paste, for example, exhibits a relatively small net

[1] In fact, the grayscale intensity matching algorithm [6] in the DMT explicitly minimizes the effect of noise in a digital image when computing relative pixel deformations.

shrinkage between 35% to 20% rh (see Table 1), which is in very good agreement with the results of Roper [3]. If we extend the analogy between C-S-H and colloidal gels, it appears that C-S-H has reached its critical point by the time it has equilibrated at 35% rh since the shrinkage of colloidal gels usually ceases at the critical point. This conclusion is supported by the fact that intense crack-like rarefactions first appeared in the sample at 35% rh. These crack-like rarefactions, which are presumably precursors to microcracks, would be expected to form in a colloidal gel at its critical point since it is a very frequent observation that gels tend to crack at their critical point [4, Ch. 8]

The 0.50 w/c paste behaved in a slightly different manner than the 0.35 w/c paste when dried below 35% rh. The net shrinkage in the 0.50 w/c sample continued to increase as the sample dried below 35% rh (see Table 1); however, intense rarefactions seem to appear at 35% rh as if the sample reached its critical point. This seeming contradiction can be resolved by noting that some coarse colloidal systems (such as sand beds or, in this case, the 0.50 w/c paste) are known to continue to shrink well past it critical point ([4], p. 468). Possibly, the 0.50 w/c paste could contain a significant proportion of some sort of interagglomerate pores (i.e., located outside the C-S-H particles) that could cause additional shrinkage when emptied below 35% rh.

3 Two Types of C-S-H

In an early model of C-S-H [6], it was shown that the reported values of nitrogen surface area in the literature can be rationalized if it is postulated that there are two types of C-S-H, one into which nitrogen can penetrate and one into which nitrogen cannot penetrate. The model, called the J-T model after its authors, does not incorporate the intuitive assumption that a higher specific surface area (SSA) is simply associated with C-S-H structure that has a more open and

accessible porous structure. Such an assumption would imply that higher measured SSA's are always associated with a greater measured volume of gel pores. However, it was recently shown [7, 8] that studies [9-11] which characterized pastes by both water and nitrogen adsorption indicate that higher nitrogen surface areas are associated with higher volumes of pores that were missed[2] by nitrogen (see Figure 5). This important observation led to the conclusion that the density of C-S-H is not constant.

In a recent analysis ([12]: Tennis, P.T. and Jennings, H.M., *A Model for two types of calcium silicate hydrate in the microstructure of Portland cement pastes*, Cem. Concr. Res. **30**, 2000, p. 855-863.) of the reported nitrogen surface areas and pore volumes it was shown that the pore structure of C-S-H can successfully be modeled with the assumption that the two types of C-S-H represent a high-density (HD) C-S-H and a low-density (LD) C-S-H. The HD C-S-H represents a more tightly packed structure into which nitrogen cannot penetrate, thereby causing the nitrogen surface area of HD C-S-H to be essentially zero. The LD C-S-H represents a more open structure that contains pores of sufficient size which allow nitrogen to partially penetrate the structure. The optimized nitrogen surface area of LD C-S-H is approximately 250 m^2/g of LD C-S-H. It is important to note that both the HD and LD C-S-H structures contain a significant amount of pores into which water can penetrate but nitrogen cannot; this aspect of the proposed structure of C-S-H (described in the next section) can thus account for the phenomenon of increasing inaccessible pore volume with increasing nitrogen surface area shown in Figure 5.

Reported in the same study [12], the optimized densities for the HD and LD C-S-H structures in the dry state were 1750 kg/m^3 and 1440 kg/m^3, respectively. These densities are

[2] The volume of these missed, or inaccessible pores, were calculated by subtracting the pore volume as measured by nitrogen with that measured by water, the latter being assumed to represent the total pore volume of the sample.

relatively low values that cannot be explained by atomic arrangement alone since the skeletal density (i.e., that of the solid network) of C-S-H is measured to be approximately 2800 kg/m^3. It can thus be concluded that the LD and HD C-S-H structures must be porous. After the porosities of these structures are calculated, the densities of LD and HD C-S-H in the saturated state become 1930 kg/m^3 and 2130 kg/m^3, respectively. As will be discussed in the next section, these values are consistent with experimental findings.

Further evidence for two densities in the C-S-H structure is provided in small angle neutron scattering (SANS) measurements on the developing surface area in cement pastes during the first three days of hydration (see Figure 6). The important observation in Figure 6 is that after about 12 to 14 hours, the surface area as detected by SANS does not continue to rise at the same rate as the amount of C-S-H that is forming; this break in linearity suggests that the C-S-H structure that is forming during the late stage (presumably HD C-S-H) possess a significantly lower surface area than the initial product (presumably LD C-S-H). It has also been postulated [13] that the early and late products could correspond to the so-called "outer product" and "inner product" types of C-S-H that have been commonly observed in backscattered scanning electron microscopy investigations.

4 Colloidal Model of C-S-H

Inspired by the recent DMT results and by the mounting evidence for two C-S-H densities, a new colloidal model of C-S-H was formulated ([7]: Jennings, H.M., *A model for the microstructure of calcium silicate hydrate in cement paste*, Cem. Concr. Res., **30**, 2000, p. 101-116.). As the name suggests, the proposed colloidal model does not model C-S-H at the atomic scale, where a relatively good understanding has been established [14]; rather, the model

attempts to quantitatively describe the very ill-defined structure of C-S-H between about 1 to 100 nm. The unique strength of the model is its ability to rationalize seemingly disparate values or surface areas, densities and pore volumes that have been reported in the literature. When values vary from one experimental technique to another, the interpretation is that they resolve different scales of the C-S-H structure. In this way, the structure of C-S-H that is proposed by the model is consistent with the widest range of experimental data possible.

The colloidal model essentially proposes C-S-H as a precipitate of roughly equiaxed colloidal particles that pack into fractal structures of high or low density. As shown in Figure 7a, the smallest particles, called the basic units, pack into "globules" that are approximately 5 nm in diameter. The globules contain approximately 18% porosity (see Table 2) and possess intraglobular pores that can only be resolved by high-resolution techniques such as small angle x-ray scattering (SAXS). Globules then pack into either the LD or HD C-S-H morphologies, thereby creating additional pores referred to as interglobular pores. The LD C-S-H (Figure 7b) is postulated to possess interglobular pores of sufficient size that allow complete detection by techniques such as small angle neutron scattering (SANS) and only partial detection by techniques such as nitrogen sorption (the latter being technique being strongly dependent on the drying procedure used in sample preparation). The interglobular pores of the HD C-S-H structure (Figure 7c), however, are proposed to be of insufficient size to be detected by SANS or nitrogen sorption; these small pores can only be detected by higher resolution techniques.

As shown in Table 2, the parameters of the model can account for a wide range of experimental and theoretical data. For example, the model can correctly predict the water content and density of C-S-H as a function of relative humidity. The model also predicts a globule radius of 2.8 nm which is consistent with SANS results [15] reporting clusters of approximately 2.5 nm.

Furthermore, the model is consistent with a wide range of surface areas measured by various techniques and with the increasing evidence of a high and low density C-S-H structure described earlier.

One of the implications of this model is that the measured surface area depends on the resolution of the experimental technique. The concept of surface area as an intrinsic material parameter thus becomes somewhat misleading. For example, it does not follow that the highest measured surface area is the correct one. It may be more important to measure the functional relationship between the measured surface area and the resolution of the applied technique. Moreover, important properties of cement paste such as shrinkage appear to be governed by the structure at the length scale of the globules rather than the smaller basic units that constitute the globules.

5 Summary

The research during the most recent period of this project has led to significant advancements in our understanding of the colloidal nature of C-S-H.

From measurements of microscopic deformations in C-S-H by a refined Deformation Mapping Technique (DMT) it was concluded that C-S-H behaves in accord with the general phenomenology of the drying of colloidal gels. In particular, C-S-H revealed large local deformations during drying, which would be indicative of a colloidal gel during drying in the constant rate period. Also, the observation of intense rarefactions in the C-S-H at its critical point coincides with much experimental and theoretical evidence that a gel is most prone to cracking at its critical point.

A reassessment of reported values of nitrogen surface area and pore volumes showed that the data can be accurately interpreted under the assumption of a high density (HD) and low density (LD) C-S-H. Recent measurements of the developing surface area of cement paste by SANS supported this hypothesis by providing direct evidence of the formation of two types of C-S-H morphologies.

Taking into account the colloidal similarities implied by the DMT and the convincing evidence for two densities in C-S-H, a colloidal model of C-S-H was formulated. The model proposes C-S-H as a colloidal precipitate of equiaxed particles that pack into fractal structure of high or low density. Predictions of density, porosity and water content at different relative humidities are very good with experimental values. More impressive, however, is the ability of the model to rationalize the disparate values of surface area that are reported by different experimental techniques.

4 Tables

Table 1. Average deformation in the w/c = 0.35 and w/c = 0.50 samples calculated by averaging the compactions and rarefactions in the field of view. The net negative deformation indicates that there is a net compaction of the sample (i.e., the sample is shrinking).

Relative Humidity	w/c = 0.35	w/c = 0.50
80%	- 0.01%	- 0.05%
75%	- 0.02%	- 0.11%
55%	- 0.08%	- 0.19%
35%	- 0.24%	- 0.32%
25%	---	- 0.51%
20%	- 0.29%	---

Table 2. Parameters of the proposed colloidal model of C-S-H.

Name of unit in structure	Radius[a] of unit (nm)	Computed density[b] ($kg\ m^{-3}$)		Surface area (m^2 / g of C-S-H)	Model porosity[c] (%)	Relative humidity condition	Measured composition	Measured density ($kg\ m^{-3}$)	Porosity based on composition[d] (%)
		Pores empty	Pores Full						
Basic Building Block	1.1	2800	2800	1000[f]	-	Dry	1.7 $CaO{\bullet}SiO_2{\bullet}1.4\ H_2O$	2800	0
Globules	2.8	2300	2480	460[g]	18	11%	1.7 $CaO{\bullet}SiO_2{\bullet}2.1\ H_2O$	2450	16
LD	8.3	1440[e]	1930	250[e]	49	Saturated	1.7 $CaO{\bullet}SiO_2{\bullet}4.0\ H_2O$	2000	42
HD	>100	1750[e]	2130	0	38	Saturated	1.7 $CaO{\bullet}SiO_2{\bullet}4.0\ H_2O$	2000	42

[a] Assuming spherical particles; using relation, $r = 3/(SSA * \rho)$ where r = radius, SSA= specific surface area, and ρ = density.
[b] Based on volume fraction of solid and pores.
[c] Calculated as $(1 - \rho_{unit} / \rho_{basic\ building\ block}) * 100$.
[d] Computed from the molar volume of dry C-S-H and the molar volume of water. The molar volume of dry C-S-H ($1.7CaO{\bullet}SiO2{\bullet}1.4H_2O$) was computed by dividing the molecular weight by the measured density to obtain a value of $6.45 \times 10^{-5}\ m^3/mol$. The molar volume of water was taken to be $1.80 \times 10^{-5}\ m^3/mol$.
[e] Values were optimized [12] by maximizing the statistical fit between reported values of nitrogen surface areas, pore volumes and capillary porosity with predicted values of the model.
[f] Based on SAXS [16, 17] data.
[g] Based on SANS data, assuming that only the LD C-S-H structure contributes to the surface area.

5 Figures

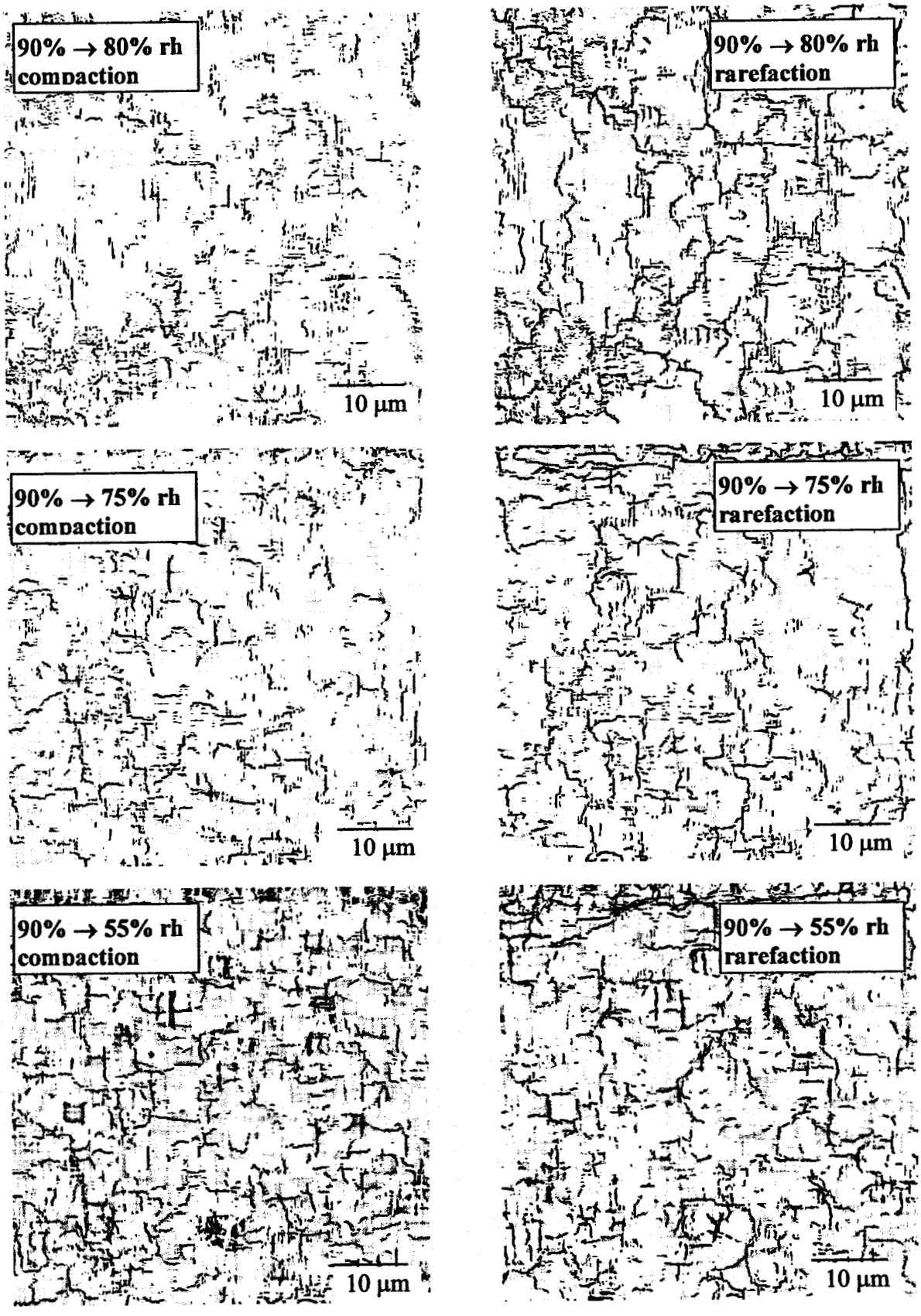

Figure 1 (continued on next page).

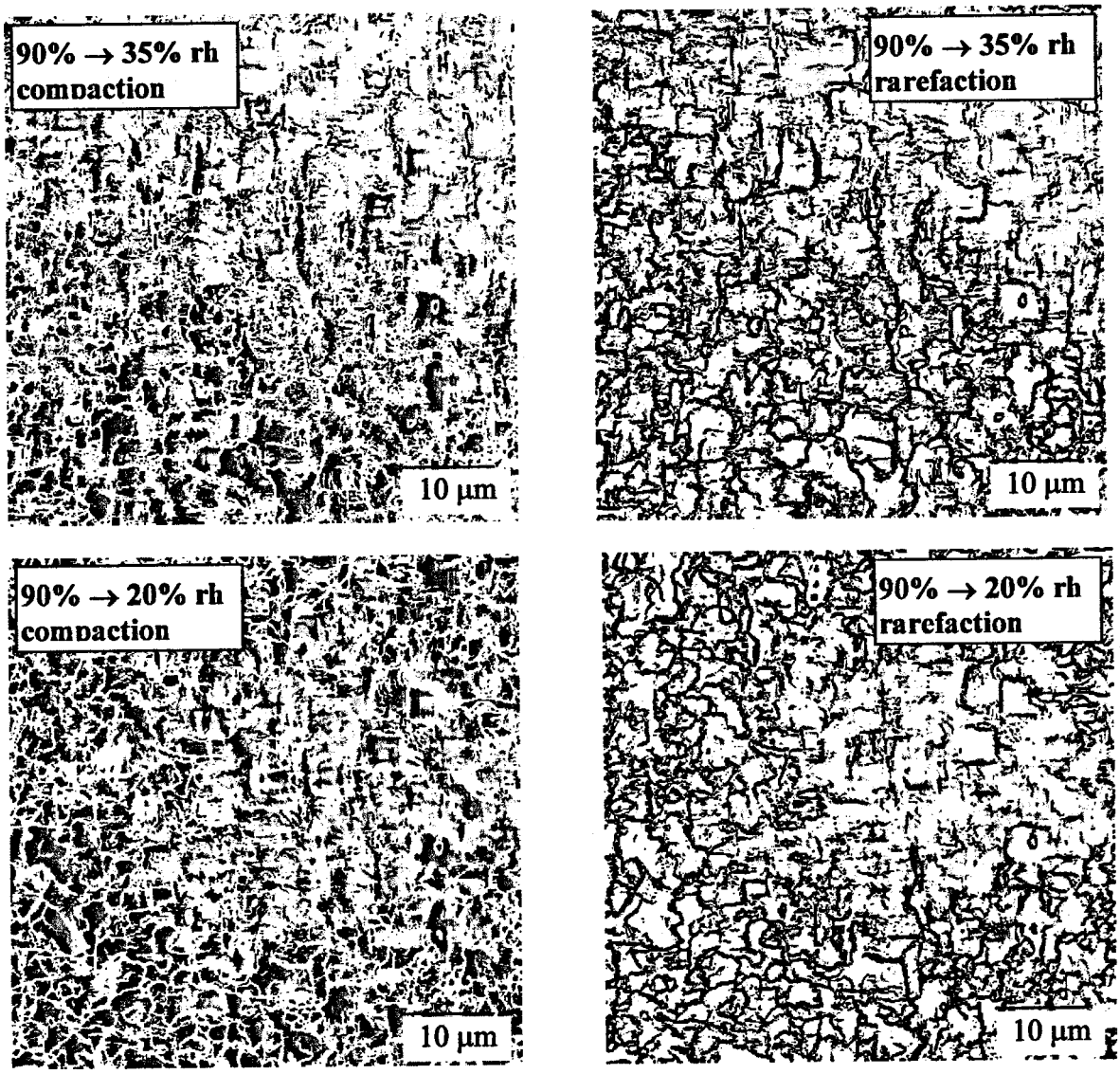

Figure 1. Compaction (left) and rarefaction (right) maps for a 7 day old cement paste of w/c=0.35 that was equilibrated at successively lower relative humidities (noted in images). Darker shades of gray indicate higher magnitudes of deformation. In all maps, the field of view is approximately 96.8 μm x 96.8 μm.

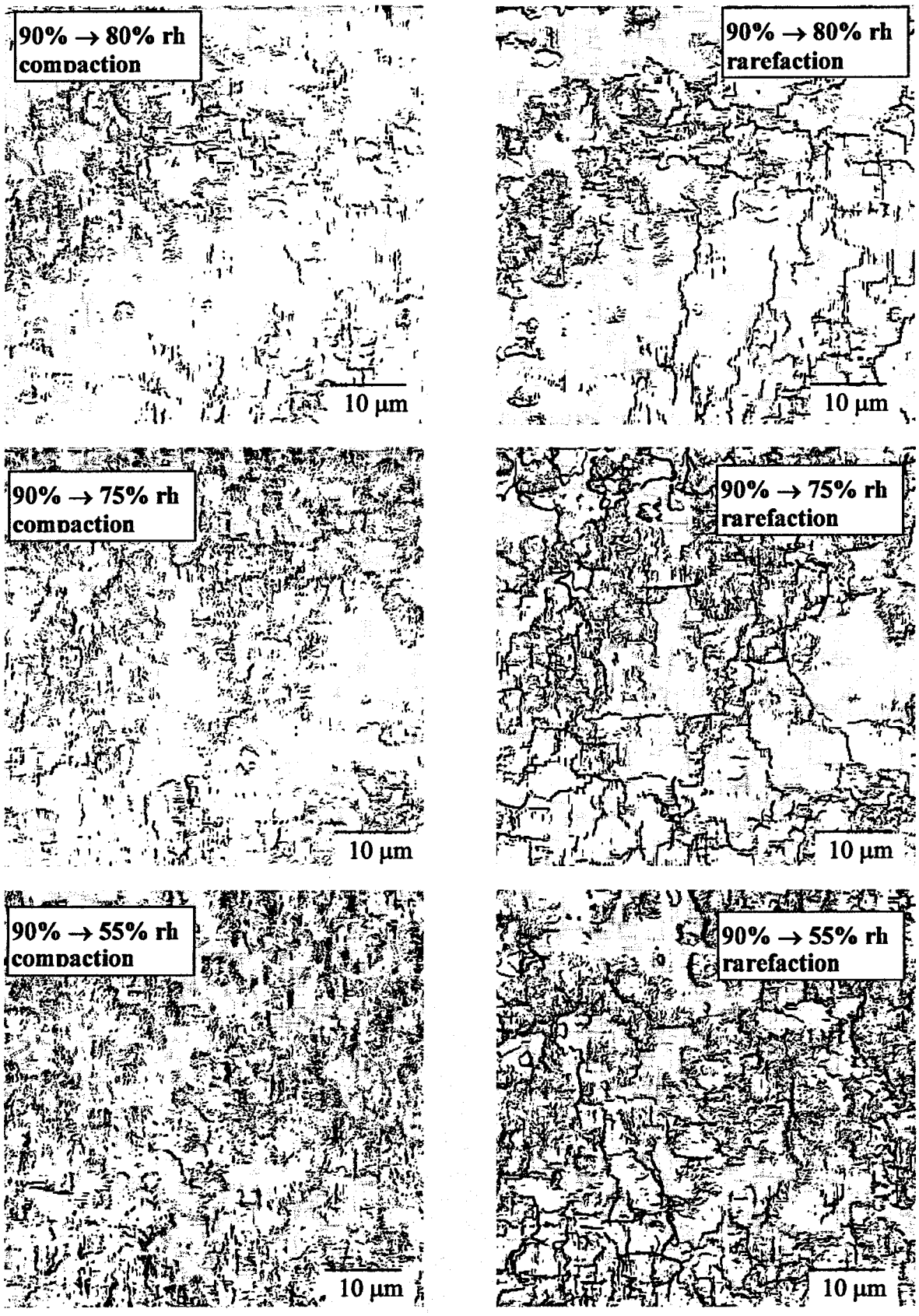

Figure 2 (continued on next page).

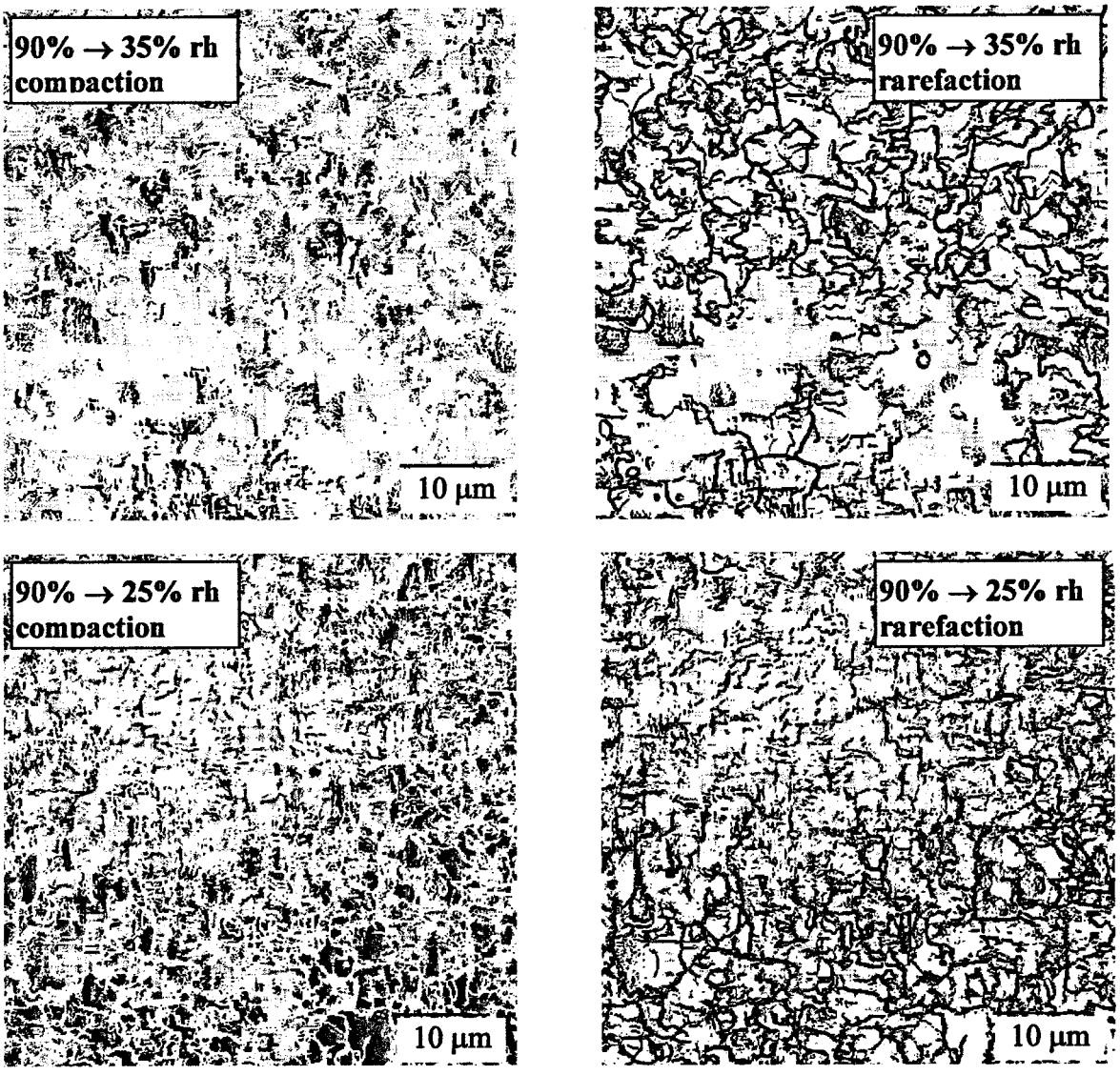

Figure 2. Compaction (left) and rarefaction (right) maps for a 7 day old cement paste of w/c=0.50 that was equilibrated at successively lower relative humidities (noted in images). Darker shades of gray indicate higher magnitudes of deformation. In all maps, the field of view is approximately 96.8 μm x 96.8 μm.

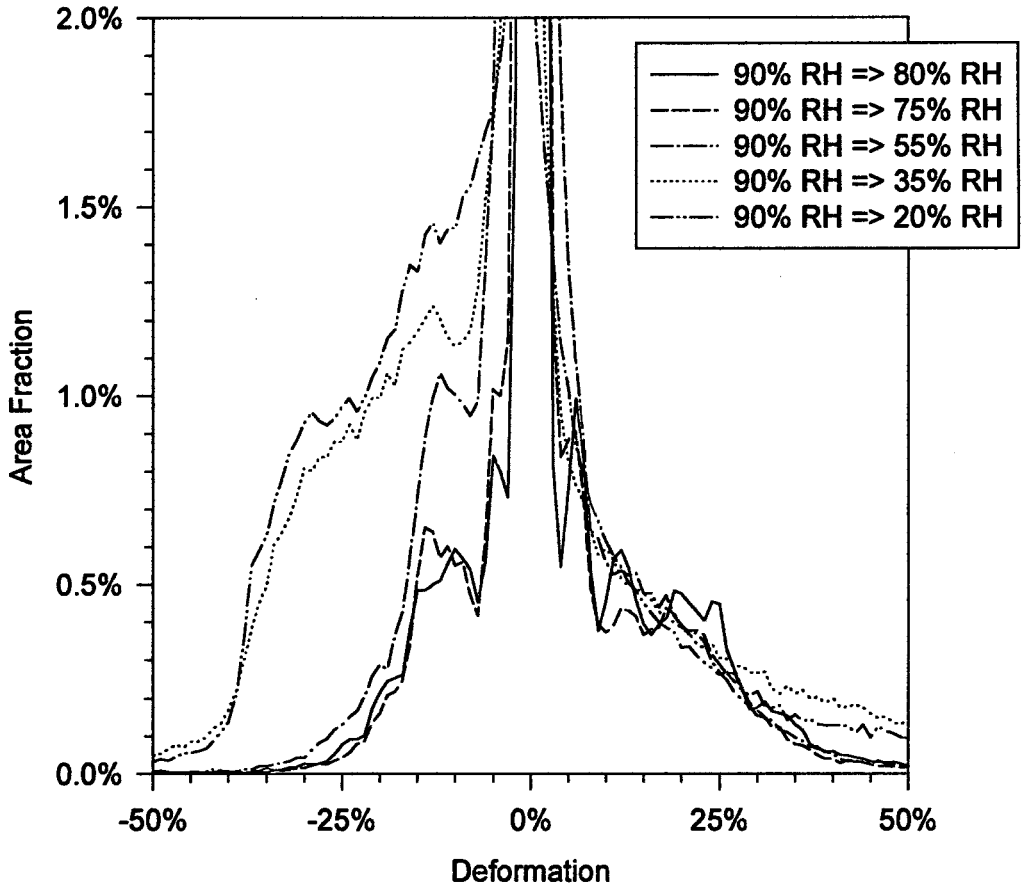

Figure 3. Deformation distributions for deformation maps shown in Figure 1 for a 7 day old sample of w/c=0.35 cement paste.

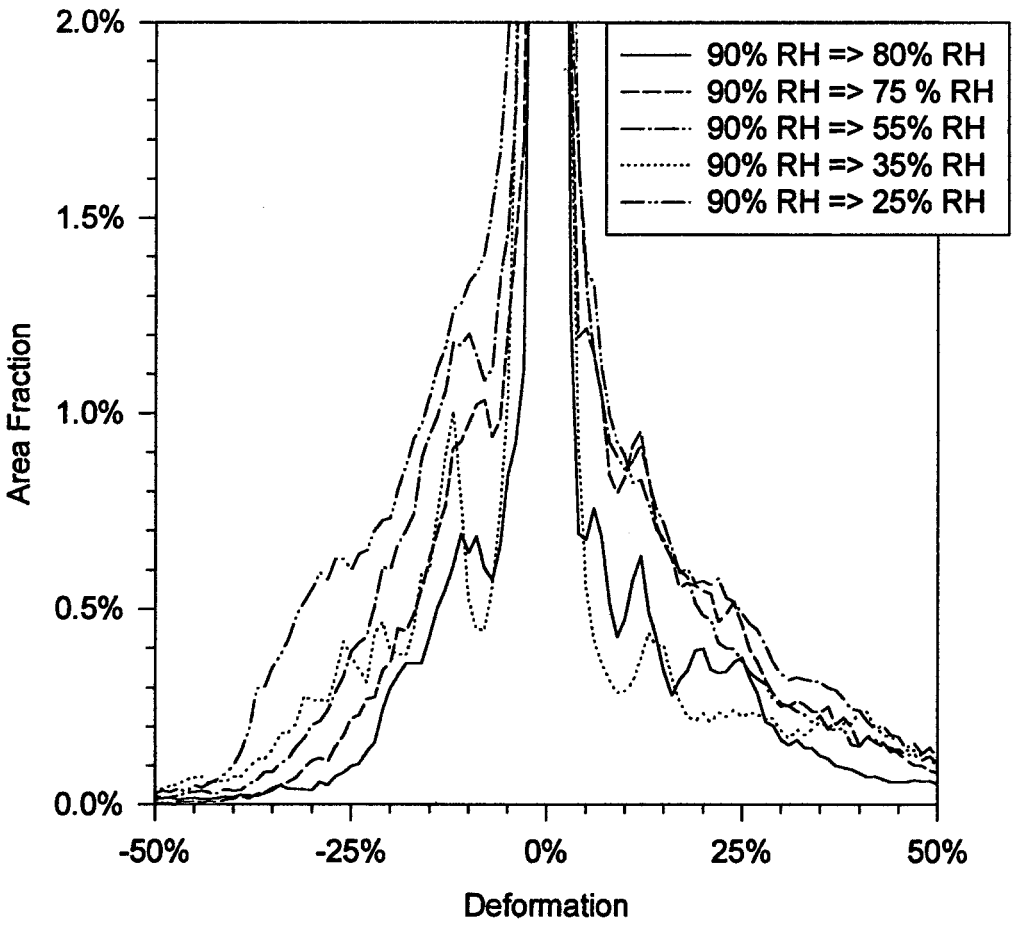

Figure 4. Deformation distributions for deformation maps shown in Figure 2 for a 7 day old sample of w/c=0.50 cement paste.

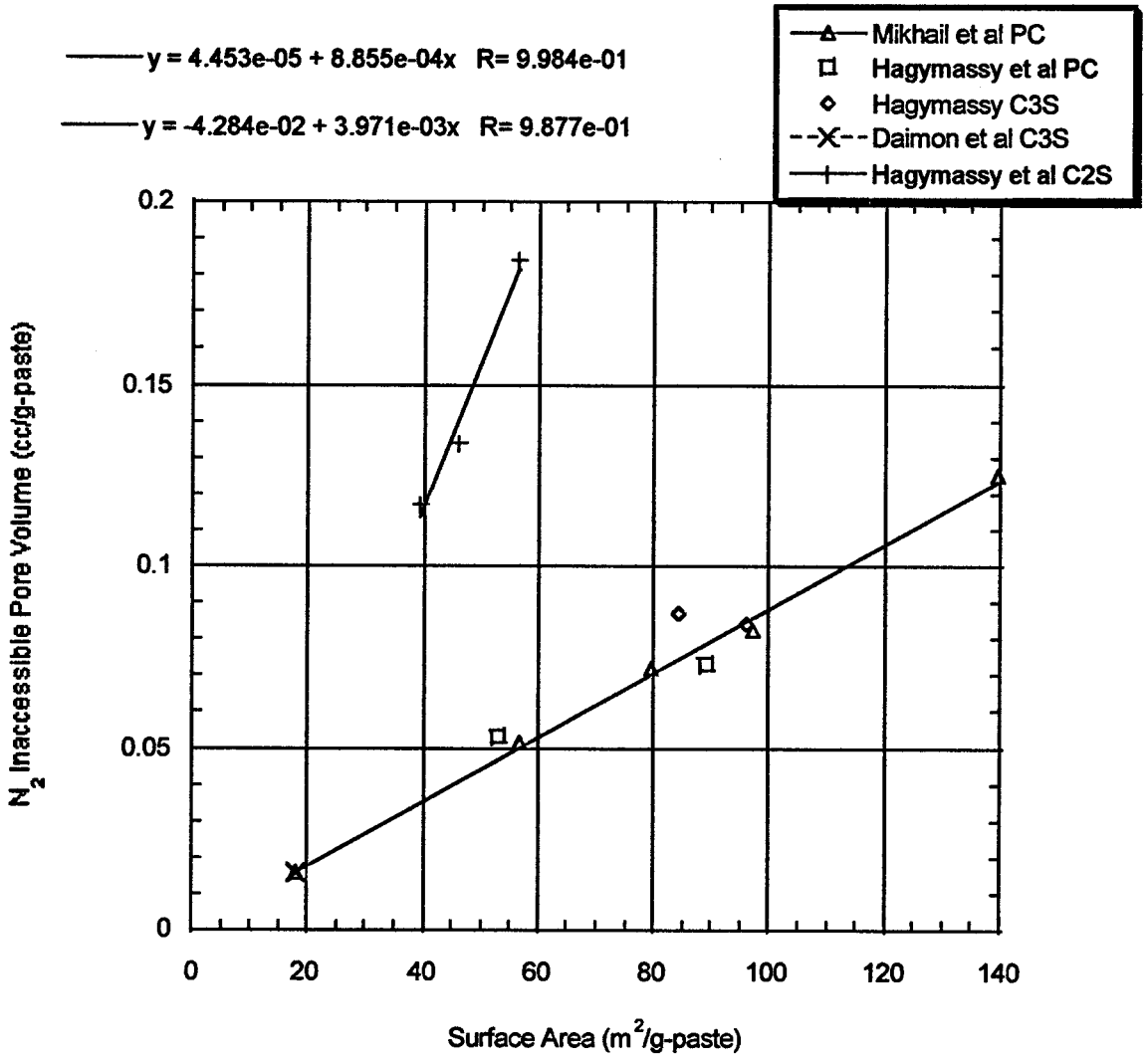

Figure 5. Quite surprisingly, higher nitrogen surface areas correlate to higher volumes of pores that are inaccessible to nitrogen. The inaccessible pore volume is the calculated as the difference between the pore volumes measured by water and nitrogen, the former being assumed to measure the entire pore volume. Data taken from Mikhail [9] for PC (Δ), Daimon et al. [11] for C_3S (X) (this point overlaps Δ at surface area ~ 20 m^2/g paste), Hagymassy et al. [10] for PC (□), C_3S (◇), C_2S (+).

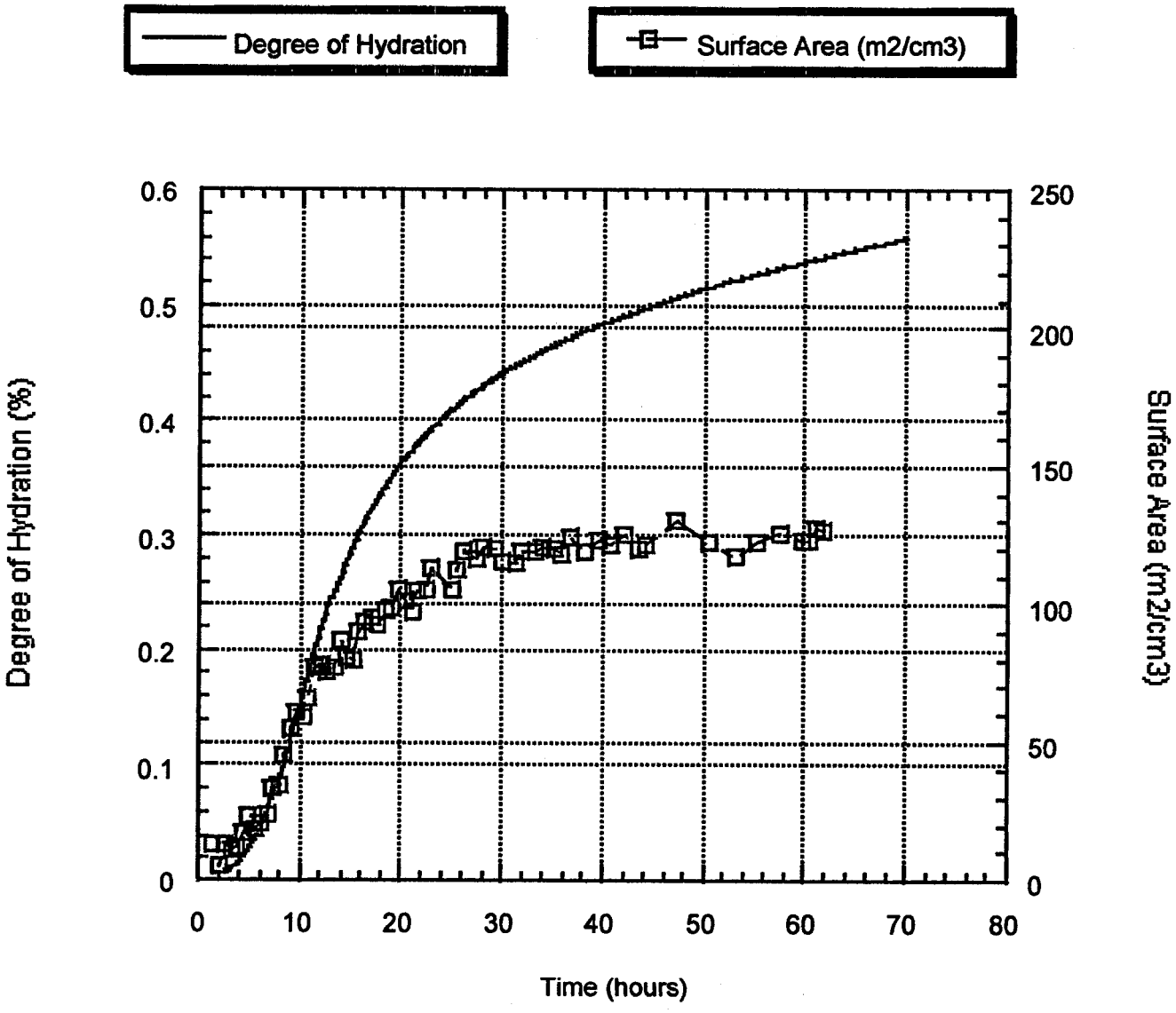

Figure 6. Degree of reaction and rate of reaction for a typical cement paste with water/cement ratio of 0.4. (after [13]). Note that the surface area is in units of m^2/volume as per original analysis, and degree of reaction is derived from original heat evolution data. The observation that after about 12-14 hrs the surface area does not continue to rise at the same rate as the amount of reaction product suggests that the product formed during the late stage has only a small surface area on average.

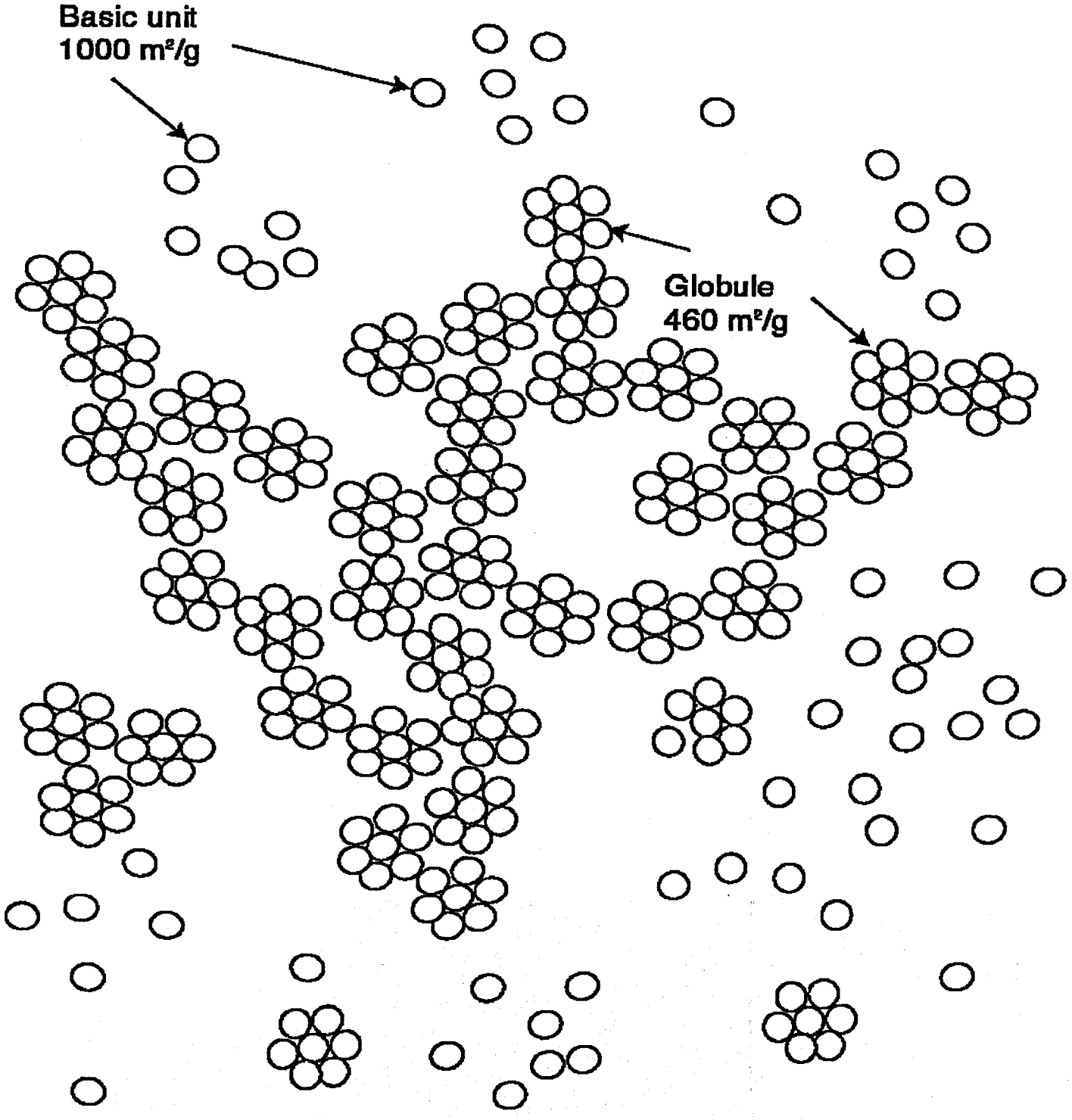

Figure 7a. A representation of semidispersed LD C-S-H formed during the first few hours of hydration. The basic unit and globules are noted in the diagram.

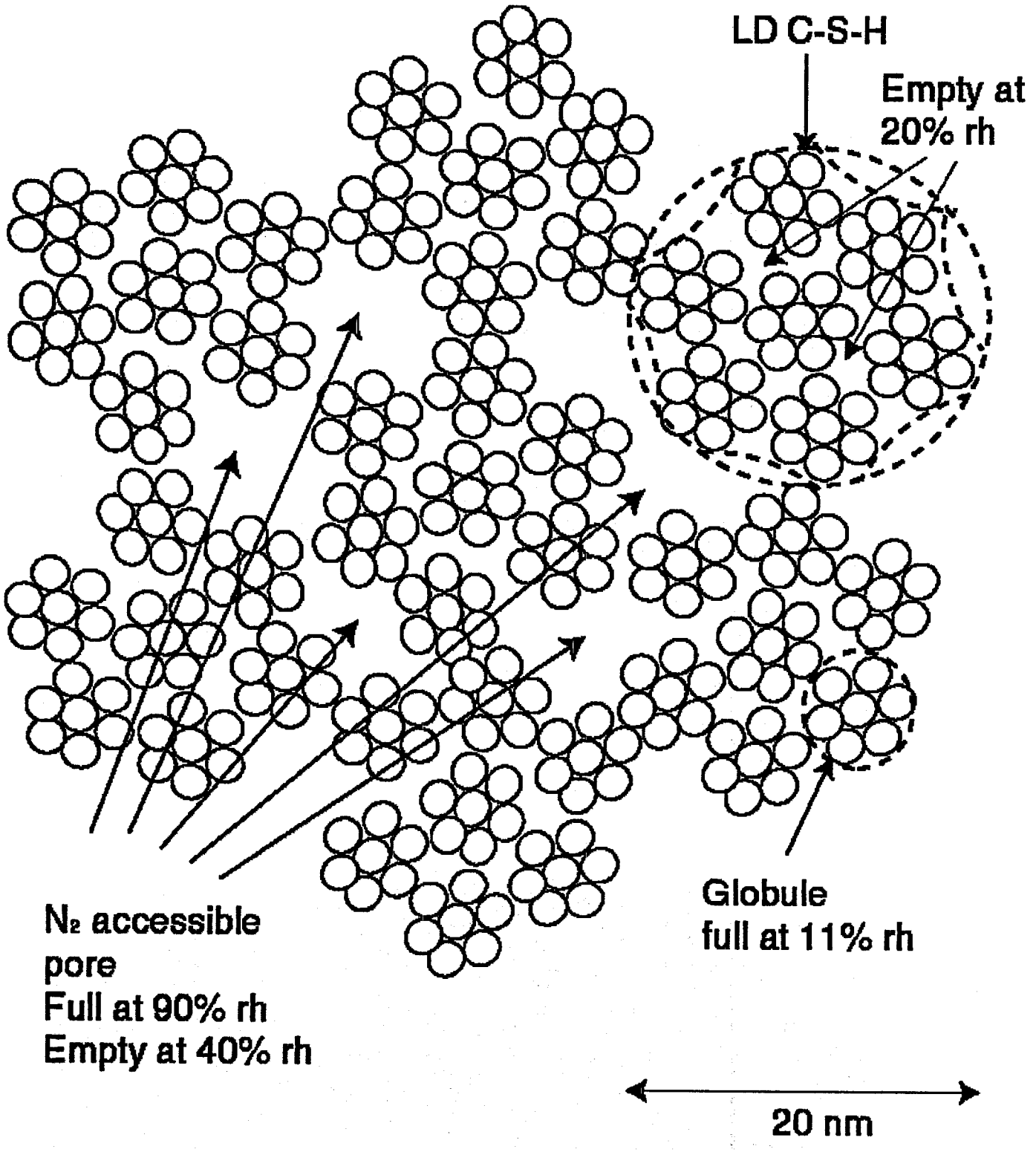

Figure 7b. A representation of LD C-S-H that is formed during the late stage of hydration and/or by drying. The LD C-S-H structure contains pores that are accessible to nitrogen.

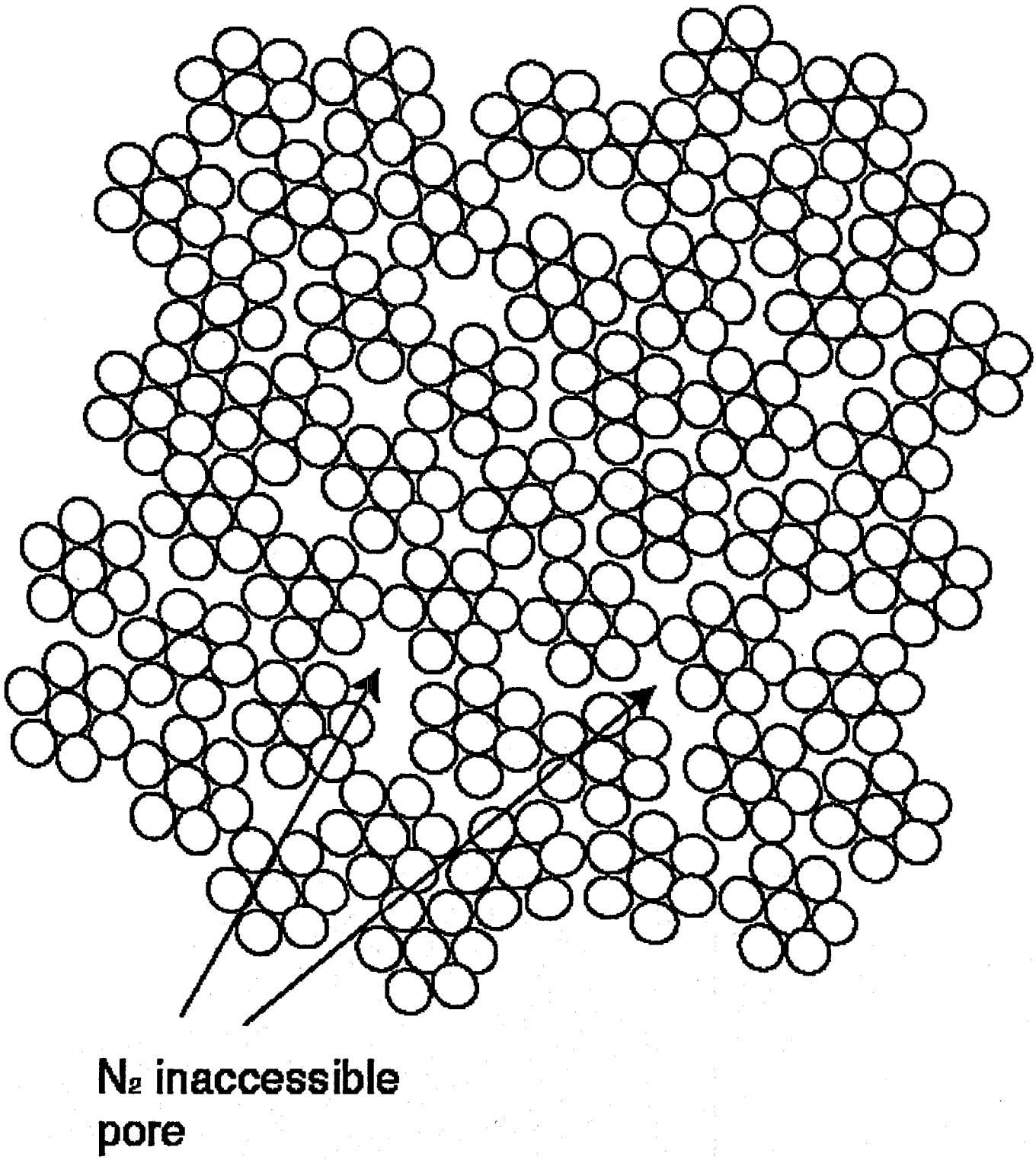

Figure 7b. A representation of HD C-S-H indicating the presence of pores that are inaccessible to nitrogen.

7 References

1. Neubauer, C.M., E.J. Garboczi, and H.M. Jennings, *Mapping microstructural drying shrinkage deformations in cement-based materials. Part I: Deformation Mapping Technique,* J. Mater. Sci., 35(22), 2000, p. 5741-5749.
2. Neubauer, C.M. and H.M. Jennings, *The Use of Digital Images to Determine Deformation throughout a Microstructure, Part II: Application to Cement Paste,* J. Mater. Sci., 35(22), 2000, p. 5751-5765.
3. Roper, H. *Dimensional change and water sorption studies of cement paste.* in *Symposium on Structure of Portland Cement Paste and Concrete,* Washington, D.C., 1966.
4. Brinker, C.J. and G.W. Scherer, *Sol-Gel Science.* 1990, NY: Academic Press, 908 pp.
5. Scherer, G.W., *Structure and properties of gels,* Cem. Concr. Res., 29, 1999, p. 1149-1157.
6. Jennings, H.M. and P.D. Tennis, *A Model for the Developing Microstructure in Portland Cement Pastes,* J. Am. Ceram. Soc., 77(12), 1994, p. 3161-3172.
7. Jennings, H.M., *A model for the microstructure of calcium silicate hydrate in cement paste,* Cem. Concr. Res., 30, 2000, p. 101-16.
8. Jennings, H.M., *Reply to the Discussion of the Paper "A Model for the Microstructure of Calcium Silicate Hydrate in Cement Paste" by Ivan Odler,* Cem. Concr. Res., 30(8), 2000, p. 1339-1341.
9. Mikhail, R.S., L.E. Copeland, and S. Brunauer, *Pore structure and surface areas of hardened Portland cement pastes by nitrogen adsorption,* Can. J. Chem., 42, 1964, p. 426-438.
10. Hagymassy, J., et al., *Pore structure analysis by water vapor adsorption III: Analysis of hydrated calcium silicates and Portland cements,* J. Coll. Interface Sci., 38(1), 1972, p. 20-34.
11. Daimon, M., et al., *Pore structure of calcium silicate hydrate in hydrated tricalcium silicate,* J. Am. Ceram. Soc., 60(3-4), 1977, p. 110-114.
12. Tennis, P.D. and H.M. Jennings, *A Model for Two Types of C-S-H in the Microstructure of Portland Cement Pastes,* Cem. Concr. Res., 30(6), 2000, p. 855-863.
13. Thomas, J.J., H.M. Jennings, and A.J. Allen, *The Surface Area of Cement Paste as Measured by Neutron Scattering - Evidence for Two C-S-H Morphologies,* Cem. Concr. Res., 28(6), 1998, p. 897-905.
14. Taylor, H.F.W., *Cement Chemistry.* 2nd ed. 1997, London: Thomas Telford, 459 pp.
15. Allen, A.J., et al., *Development of the Fine Porosity and Gel Structure of Hydrating Cement Systems,* Phil. Mag. B, 56(3), 1987, p. 263-268.
16. Winslow, D.N., J.M. Bukowski, and J.F. Young, *The Early Evolution of the Surface of Hydrating Cement,* Cem. Concr. Res., 24(6), 1994, p. 1025-1032.
17. Winslow, D.N. and S. Diamond, *Specific Surface of Hardened Cement Paste as Determined by Small-Angle X-Ray Scattering,* J. Am. Ceram. Soc., 57(5), 1974, p. 193-197.